

Enhanced Ferromagnetic Ordering in $\text{GdBaCo}_2\text{O}_{5.5+}$ Films on SrTiO_3 (001) Substrate

G. Y. Wang, X. Y. Zhou, R. K. Zheng, Y. M. Hu, H. L. W. Chan and Y. Wang
 Department of Applied Physics and Materials Research Center,
 the Hong Kong Polytechnic University,
 Hong Kong SAR, China

(Dated: April 1, 2024)

The authors investigated the structure and properties of $\text{GdBaCo}_2\text{O}_{5.5+}$ thin films epitaxially grown on SrTiO_3 (001) single crystal substrates. The thin films were found to have a notable remnant magnetization above room temperature, which is much higher than that observed in bulk material. Transmission electron microscopy and x-ray diffraction patterns reveal that phase separation occurs in these films, and the phase responsible for the enhanced ferromagnetic order is a-oriented. The enhanced ferromagnetic order is attributed to the enhanced orbital order of Co^{3+} in CoO_5 pyramids, and the disappearance of ferromagnetic to antiferromagnetic transition is explained the stabilization of higher spin state of Co^{3+} in CoO_6 octahedra.

PACS numbers: 68.37.-d, 75.70.-i, 68.37.Lp

I. INTRODUCTION

Perovskite-related cobalt oxides, e.g. $\text{R}_1 \times \text{A}_x \text{CoO}_3$ (R = rare earth metals, $\text{A} = \text{Ca}, \text{Sr},$ and Ba), have recently attracted much attention due to their interesting physical properties such as colossal magnetoresistance¹, large thermoelectric efficiency², and spin-state transition^{3,4,5,6}. In these oxides, CoO_6 octahedron is a fundamental structure in which the Co ions may have different valences (Co^{2+} , Co^{3+} and Co^{4+}) and spin states (for Co^{3+} : high spin state, HS, $t_{2g}^4 e_g^2$, $S=2$; intermediate spin state, IS, $t_{2g}^5 e_g^1$, $S=1$; low spin state, LS, $t_{2g}^6 e_g^0$, $S=0$). Since the Hund coupling energy J_H is comparable to the crystal-field splitting energy E in some doping levels, the spin state of Co ions can be converted by stimulation of some external variables such as temperature^{3,4} and pressure⁶, which modifies the value of J_H / E .

Very recently, great interests have been paid to layered cobalt oxides $\text{RBaCo}_2\text{O}_{5.5+}$,^{7,8,9,10,11,12,13,14,15,16} where R^{3+} and Ba^{2+} ions locate in alternating planes along c-axis due to their large mismatch in ion radii. In $\text{RBaCo}_2\text{O}_{5.5+}$, the oxygen content can be significantly modified by different annealing process, which tunes the nominal valence of cobalt from 2.5+ to 3.5+. The oxygen vacancies always appear in rare-earth planes^{7,8}, and turns two neighboring CoO_6 octahedra to pyramids. Among these layered cobalt oxides, $\text{GdBaCo}_2\text{O}_{5.5+}$ (GBCO) has been well studied^{7,13,14,15,16} and multiple phase transition has been observed. In none doping $\text{GdBaCo}_2\text{O}_{5.5}$, half of Co^{3+} ions are in octahedra and the others are in pyramids. The oxygen vacancies were ordered in a row running along a-axis. A spin-state transition is observed at 360 K, associated with a metal-insulator transition, where the spin state of Co^{3+} ions

in octahedra change from HS to LS with decreasing temperature while those in pyramid remains IS.¹⁵ Taskin et al. found that the IS Co^{3+} ions in pyramids formed ferromagnetic (FM) two-leg ladders running along a-axis due to orbital ordering, and the spins exhibit a strong Ising-like anisotropy that all the spins point to a-axis¹⁵. The ground state of GBCO is antiferromagnetic (AFM) and changes to FM state at 260 K due to the appearance of $\text{Co}^{2+} / \text{Co}^{4+}$ pairs or the LS to IS/HS transition of Co^{3+} in some of the octahedra. At 300 K the compound undergoes a phase transition from FM state to paramagnetic state, due to the destroyed FM ladders by thermal fluctuation¹⁵.

Although many studies have been performed on bulk material, few works^{17,18} has been done on the substrate-induced strain effects for $\text{RBaCo}_2\text{O}_{5.5+}$ thin films. In this report, we fabricated epitaxial GBCO films on SrTiO_3 (001) substrates and found a strain-enhanced FM order at high temperature (430 K), which is seldom observed in perovskite cobalt oxides.

II. EXPERIMENT DETAILS

A ceramic target of GBCO was prepared by the solid-state reaction method in air with stoichiometric Gd_2O_3 , BaCO_3 and Co_3O_4 . X-ray diffraction (XRD) measurement shows that the GBCO ceramic target is single phase. GBCO thin films with thickness of 40 nm and 100 nm were deposited on SrTiO_3 (001) single crystal substrates by pulsed laser ablation technique. During deposition, the substrate temperature was kept at 700 °C and the oxygen pressure was kept at 27 Pa. After deposition, the films were cooled to room temperature in 1000 Pa O_2 . As-grown 40 nm film (labeled A1) were post-annealed in coating oxygen at 400 °C for three hours (labeled A2), and then in air at 900 °C for 1 hour (labeled A3). The structure of the thin films was characterized by a Discover D8 x-ray diffractometer equipped with

Corresponding author; Electronic address:
 apywang@inet.polyu.edu.hk

Cu K radiation and a Joel 2010F Transmission electron microscopy (TEM). Vibrating sample magnetometer (VSM) and superconducting quantum interference device (SQUID) magnetometer were employed in the magnetic characterizations.

III. RESULT AND DISCUSSION

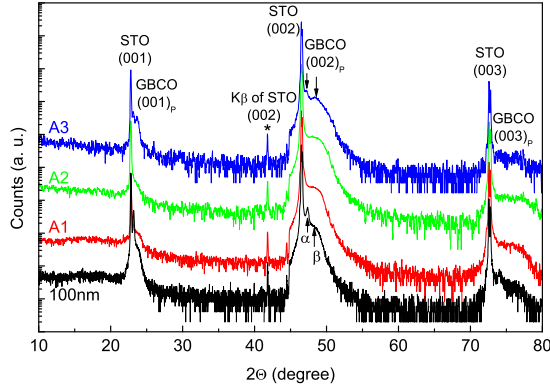


FIG. 1: X-ray diffraction patterns of the thin films with different thickness and heat treatments. The arrows indicate two different peaks from thin film.

The GBCO ceramic was found to have an orthorhombic structure with lattice parameters $a = 3.88 \text{ \AA}$, $b/2 = 3.915 \text{ \AA}$, and $c/2 = 3.77 \text{ \AA}$, consistent with that reported in literature¹⁵. Fig. 1 shows the XRD patterns of thin films with different thickness and heat treatments. For 100 nm film, a peak with strong intensity is found at $2\theta = 47.3^\circ$, corresponding to the out-of-plane lattice parameter (with perovskite structure) 3.85 \AA of thin film. A hump with weaker intensity can be seen at $2\theta = 48.3^\circ$, indicating smaller out-of-plane lattice parameter of 3.77 \AA . This suggests the possible phase separation in this thin film. It should be pointed out that no peak is observed at $2\theta = 12^\circ$ (corresponding to $d = 7.8 \text{ \AA}$), which may be caused by the weaker intensity of this peak. In $\text{TbBaCoO}_{5.5+}$ thin films this peak also disappeared but appeared after slowly cooling down from high temperature¹⁷, indicating the sensitivity of this peak to the heat treatment in thin films. For 40 nm films, it can be seen that all the thin films show hump at about 48.3° , reducing the out-of-plane lattice parameter of 3.77 \AA . The hump shows only small shift among A1, A2 and A3. Comparing with 100 nm film, the peak at 47.3° disappears in A1 and A2, but presents in A3. This indicates that phase separation is also present in high-temperature treated A3, which will be confirmed by high-resolution TEM (HRTEM) images in the last figure. From now on we define phase α to the peak with longer out-of-plane axis (smaller 2θ) and phase β to the hump with shorter out-of-plane axis (larger 2θ).

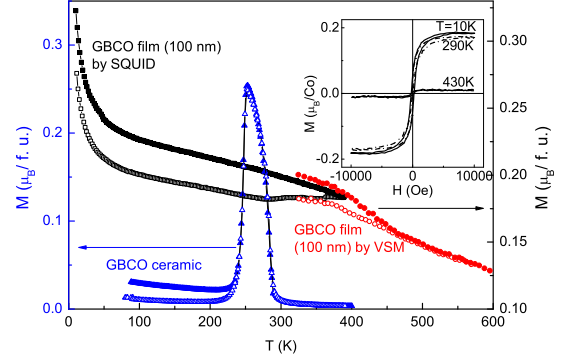


FIG. 2: Temperature dependence of magnetization for the GBCO ceramic sample and 100 nm thin film at $H = 1000 \text{ Oe}$. Inset shows the ferromagnetic component of magnetization for 100 nm thin film at 10 K, 290 K, and 430 K (the diamagnetic and paramagnetic signals are subtracted).

Figure 2 shows the temperature dependence of magnetization for the GBCO thin film (100 nm) and ceramic target. In the ceramic, a FM order emerges at 288 K with decreasing temperature, but soon changes to AFM order at 255 K. This is a typical characteristic of GBCO with c/a close to 0.¹⁵ The magnetization of thin film (squares for the data taken by SQUID and circles for those taken by VSM), however, is quite different. In thin film, the FM-AFM transition disappeared, which could be induced by oxygen deficiency¹⁵ or substrate-induced strain effect. We note that a remnant magnetization can be seen even at 430 K, which is higher than that reported in GBCO ceramic and single-crystal^{7,13,14,15} with any oxygen content. This is an unusual behavior in perovskite-related cobalt oxides of which the Curie temperature is usually not higher than 300 K^{7,8,9,10,11,12,13,14,15}. The inset of Fig. 2 shows the field dependence of magnetization of the thin film at 10, 290 and 430 K, respectively. The $M(H)$ curves confirm that the FM order emerges at about 430 K. It should be pointed out that all paramagnetic and diamagnetic moments have been subtracted and only the FM moment is presented in the $M(H)$ curves. From this figure, we can see that the FM order in thin film is not only expanded to low temperature, but also to high temperature comparing with ceramic sample.

Temperature and field dependence of magnetization of 40 nm thin film is shown in Fig. 3. The as-grown thin film A1 shows a FM behavior below 350 K, which is also higher than that in bulk material. In GBCO bulk material, the annealing at 400 °C in 1 bar oxygen will increase the oxygen content ($5+$) to a higher value (> 5.53), which suppresses the FM order to lower temperature¹⁵. In thin film, this effect is even much notable: the spontaneous magnetization in A2 disappears above 77 K. Either higher sensitivity of FM order to oxygen content in thin film, or higher oxygen content in thin film, should be responsible to this. The annealing at 900 °C in air and cooling to room tempera-

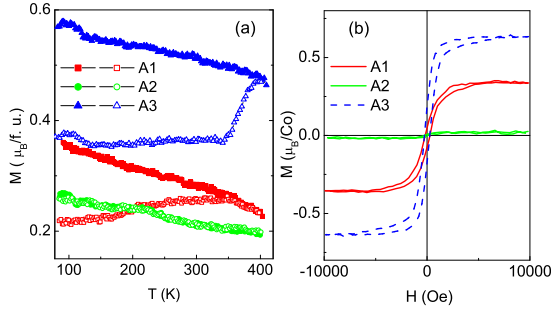


FIG. 3: (a) Temperature dependence of magnetization at $H = 1000$ Oe for A1, A2 and A3. Open symbols for zero-field-cooled data and close symbols for field-cooled data. (b) Field dependence of FM magnetization at room temperature (the diamagnetic and paramagnetic signal are subtracted).

ture with furnace is believed to reduce the oxygen content to 5.5 in bulk materials¹⁵, but in In , this procedure has another effect: relaxation of strain comes from substrate. In A3, the spontaneous magnetization recovers, and the Curie temperature shift to higher than 400 K. The x-ray diffraction pattern in Fig. 1 also shows an additional peak comparing to A1 and A2, which is the result of strain relaxation. The $M(H)$ curves in Fig. 3 (b) confirm the remnant magnetization above room temperature in A1 and A3, and also the disappearance of remnant magnetization above room temperature in A2.

Fig. 4 (a) shows the HRTEM cross-section image taken from the surface of 100 nm In . Doubled lattice period is observed in in-plane direction but not in out-of-plane direction. The fast Fourier transform (FFT) result of this area, shown in the inset of Fig. 4 (a), confirms this observation. It has been mentioned above that in GBCO only a-axis is not doubled comparing with perovskite lattice, which enable us to identify different axis in GBCO In . So the a-axis of GBCO In in Fig. 4 (a) is out of plane. Some literatures also reported the superstructure along a-axis due to atom displacement,²⁰ but the intensity of superstructure reflection they observed is so low (2-4 orders lower than fundamental ones) that we won't see it even in our FFT results. Fig. 4 (b) shows the HRTEM cross-section image of A3, where two domains are present in In . For the domain near the substrate- In interface, the in-plane lattice is not doubled, but for the domain near the In surface, the out-of-plane lattice is not doubled. The FFT results of different areas are shown in Fig. 4 (c). For the same reason mentioned above, we can identify a-axis of different domains, which is schematically shown in Fig. 4 (c). In fact, the domain with in-plane a-axis is also found near the interface of 100 nm In and in the whole In of A1, but the domain with out-of-plane a-axis is not found in A1. The HRTEM results are consistent with XRD patterns in Fig. 1, if we regard phase α to the domain with out-of-plane a-axis and phase β to the domain with in-plane a-axis.

One may ask that why phase α presents, since a-axis is much closer to the lattice parameter of STO substrate than c-axis. Here is a phenomenology explanation. If we just consider the lattice parameter, c-axis will surely present out-of-plane in order to reduce the elastic energy of In , since $a = 3.88 \text{ \AA}$ and $b/2 = 3.92 \text{ \AA}$ is much closer to the STO lattice parameter (3.906 \AA) comparing with $c/2 = 3.77 \text{ \AA}$. But as mentioned by Taskin et al.¹⁵, the oxygen atom diffusion along c-axis is negligible in comparison of ab plane in GBCO. And the equilibrium oxygen content is very sensitive to the temperature and oxygen pressure. During the deposition and annealing, different heat treatments are surely applied to the In . a or b-axis lies out-of-plane is a good choice to favor the oxygen diffusion during different heat treatment. But b will not present out-of-plane considering that b-axis is the only one larger than that of STO substrate. So, in A1, only β phase is present due to strain restriction comes from substrate; but in 100 nm In , α phase is present near the interface and β phase is present near the surface of In due to the relaxation of strain with increasing thickness. Phase α is also present in A3, where the high-temperature annealing may enhance the relaxation of strain by creating more defects. The defects can be seen near the domain boundary, and even in phase β .

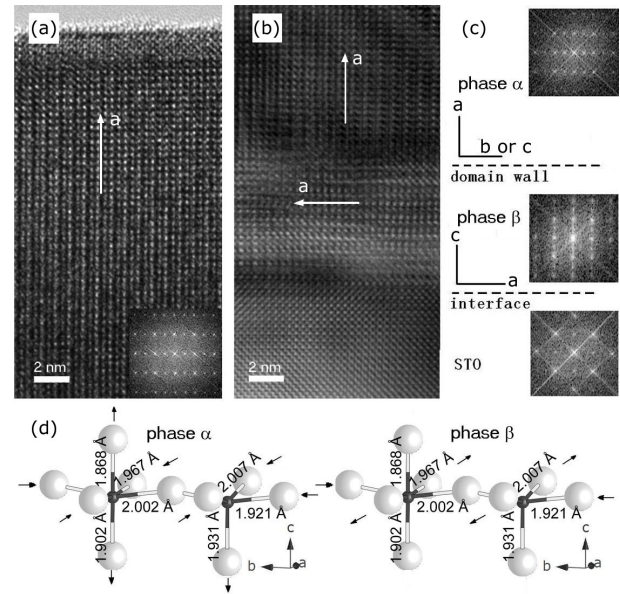


FIG. 4: (a) HRTEM image taken from the surface of 100 nm In . inset shows the FFT result of this area. (b) HRTEM image taken from the interface of A3. Two domains can be clearly seen in the In . The FFT results of different areas in (b) are shown in (c). (d) The strain state in phase α and β .

Now we should explain the origin of enhanced FM order, which is expanded to both low temperature and high temperature. Based on the XRD results in Fig. 1, a and b are compressed, c is elongated in phase α ; a is elongated and b is compressed, but c is almost unchanged in phase β . These strain state are indicated by arrows in Fig. 4.

4 (d), where only CoO_6 octahedron and CoO_5 pyramid are present. The bond length are reproduced from the structure information in literature.¹⁹ First, about the disappearance of AFM phase at low temperature. In bulk material, the AFM-FM transition is caused by the appearance of e_g electron of Co^{3+} in octahedra, which is induced by either the appearance of $\text{Co}^{2+}/\text{Co}^{4+}$ pairs or the LS to IS/HS transition of Co^{3+} in some of the octahedra with increasing thermal excitation. But in In , as shown in Fig. 4 (d), the strain in phase and phase will tune the octahedra to less distorted one, decrease the crystal field splitting energy E and stabilize higher spin state of Co^{3+} in it. The appearance of e_g electron of Co^{3+} in octahedra will surely kill the AFM phase¹⁵ in all the In s. Second, about the enhanced FM order at high temperature. In bulk material, the AFM orbital order in two-leg ladders induces FM order inside ladders due to Goodenough-Kanamori rules. But these ladders will be killed by increasing thermal fluctuation, which is the reason of FM order disappears at high temperature. In In , we can't identify the local distortion of pyramids (including the bond length and bond angle) in this study, but our experimental results indicate that the biaxial strain on the pyramids, as shown in Fig. 4 (d), has positive effect on the orbital ordering in these two-leg ladders. Especially the strain in phase can increase the orbital-ordering temperature to a much higher one. Enhanced FM order to high temperature was also

observed in GBCO-In s on $(\text{LaAlO}_3)_{0.3}(\text{Sr}_2\text{AFeO}_6)_{0.7}$ with $a = 3.86 \text{ \AA}$, where the same strain type as phase can be found (data not shown here). Pressure effect on the magnetic properties of GBCO single crystal is needed to confirm our supposition.

IV. CONCLUSION

In summary, epitaxial GBCO-In s were grown on STO (001) single crystal substrates. XRD and TEM patterns reveal the phase separation phenomena in In . The magnetic behavior of the In s shows large difference from the bulk material: AFM-FM transition disappears and Curie temperature is shifted to a much higher temperature. The origin of this enhanced FM order is due to the substrate-induced strain, and a-oriented phase contributes much more to the enhanced FM order.

ACKNOWLEDGMENTS

This work was supported by the Hong Kong Polytechnic University Postdoctoral Scheme (G-YXOC) and internal funding (L-BB84). The support from the Center for Smart Materials is also acknowledged.

-
- ¹ G. Briceo, H. Y. Chang, X. D. Sun, P. G. Schultz, and X. D. Xiang, *Science* **270**, 273 (1995).
- ² I. Terasaki, Y. Sasago, and K. Uchinokura, *Phys. Rev. B* **56**, R12685 (1997).
- ³ M. A. Senaris-Rodriguez and J. B. Goodenough, *J. Solid State Chem.* **116**, 224 (1995).
- ⁴ S. Tsubouchi, T. Kiyomoto, M. Itoh, P. Ganguly, M. Oguni, Y. Shimoyama, Y. Mori, and Y. Ishii, *Phys. Rev. B* **66**, 052418 (2002).
- ⁵ T. Fujita, T. Miyashita, Y. Yasui, Y. Kobayashi, M. Sato, E. Nishibori, M. Sakata, Y. Shimoyama, N. Igawa, Y. Ishii, K. Kakurai, T. Adachi, Y. Ohishi, and M. Takata, *J. Phys. Soc. Jpn.* **73**, 1987 (2004).
- ⁶ I. Fita, R. Szymczak, R. Puzniak, I. O. Troyanchuk, J. Fink-Finowicki, Ya. M. Mukovskii, V. N. Varyukhin, and H. Szymczak, *Phys. Rev. B* **71**, 214404 (2005).
- ⁷ C. Frontera, A. Caneiro, A. E. Carrillo, J. Oro-Sole and J. L. Garcia-Munoz, *Chem. Mater.* **17**, 5439 (2005); C. Frontera, J. L. Garcia-Munoz, A. E. Carrillo, M. A. Garcia-Randa, I. M. Argiolaki, A. Caneiro, *Phys. Rev. B* **74**, 054406 (2006).
- ⁸ A. Maignan, C. Martin, D. Pelloquin, N. Nguyen, and B. Raveau, *J. Solid State Chem.* **142**, 247 (1999).
- ⁹ S. Roy, I. S. Dubenko, M. Khan, E. M. Condon, J. Craig, N. Ali, W. Liu, B. S. Mitchell, *Phys. Rev. B* **71**, 024419 (2005).
- ¹⁰ E. Pomjakushina, K. Conder, and V. Pomjakushin, *Phys. Rev. B* **73**, 113105 (2006).
- ¹¹ Md. Motin Seikh, Ch. Simon, V. Caignaert, V. Pralong, M. B. Lepetit, S. Boudin, and B. Raveau, *Chem. Mater.* **20**, 231 (2008).
- ¹² D. D. Khalyavin, D. N. Argyriou, U. Amann, A. A. Yaremchenko and V. V. Kharton, *Phys. Rev. B* **75**, 134407 (2007).
- ¹³ I. O. Troyanchuk, N. V. Kasper, D. D. Khalyavin, H. Szymczak, R. Szymczak, and M. Baran, *Phys. Rev. Lett.* **80**, 3380 (1998).
- ¹⁴ M. Respaud, C. Frontera, J. L. Garcia-Munoz, Miguel Angel Garcia-Randa, B. Raquet, J. M. Broto, H. Rakoto, M. Goiran, A. Llobet, and J. Rodriguez-Carvajal, *Phys. Rev. B* **64**, 214401 (2001).
- ¹⁵ A. A. Taskin, A. N. Lavrov, and Y. Ando, *Phys. Rev. Lett.* **90**, 227201 (2003); A. A. Taskin, A. N. Lavrov, and Y. Ando, *Phys. Rev. B* **71**, 134414 (2005); A. A. Taskin, A. N. Lavrov, and Y. Ando, *Phys. Rev. B* **73**, 121101 (R) (2006); A. A. Taskin, A. N. Lavrov, and Y. Ando, *Progress in Solid State Chem.* **35**, 481 (2007).
- ¹⁶ X. S. Wu, H. L. Zhang, J. R. Su, C. S. Chen, and W. Liu, *Phys. Rev. B* **76**, 094106 (2007).
- ¹⁷ N. V. Kasper, P. Wochner, A. Vignante, H. Dosch, G. Jakob, H. D. Carstanjen, and R. K. Kremer, *J. Appl. Phys.* **103**, 013907 (2008).
- ¹⁸ Z. Yuan, J. Liu, C. L. Chen, C. H. Wang, X. G. Luo, X. H. Chen, G. T. Kim, D. X. Huang, S. S. Wang, A. J. Jacobson, and W. Donner, *Appl. Phys. Lett.* **90**, 212111 (2007).
- ¹⁹ C. Frontera, J. L. Garcia-Munoz, A. Llobet, and M. A. Garcia-Randa, *Phys. Rev. B* **65**, 180405 (R) (2002).
- ²⁰ Yu. P. Chemenkov, V. P. Plakhty, V. I. Fedorov, S. N. Barib, S. V. Shiryayev, and G. L. Bychkov, *Phys. Rev. B*

71, 184105 (2005).